01

Ab initio Calculations of the Electronic Structure of the Doublet and Quartet States of the Rubidium Trimer

© E.A. Bormotova, A.S. Likharev, A.V. Stolyarov

Department of Chemistry, Moscow State University,
119991 Moscow, Russia

e-mail: bormotova.e.a@gmail.com, avstol@gmail.com

Received June 26, 2023
Revised September 13, 2023
Accepted September 13, 2023

Systematic quantum chemical calculations were performed for the ground and a number of low-lying electronically excited doublet and quartet states of the rubidium trimer molecule. The obtained potential energy surfaces (PES), spin-orbit couplings (SOC) and electronic transition dipole moments (ETDM) can be useful for optimizing paths for laser synthesis, cooling and manipulation of stable ensembles of Rb_3 molecules at ultralow temperatures. Ab initio calculations of the electronic structure of the homonuclear Rb_3 molecule, in linear, isosceles triangle and equilateral triangle geometries, were performed using the multi-reference configuration interaction method, taking into account single and double excitations (MR-CISD) and with explicit dynamic correlation of only the three valence electrons. The structure of each atom was approximated using a nine-electron effective core potential (ECP28MDF), and molecular orbitals (MOs) were optimized using the spin averaged (over doublet and quartet states) multi-configuration self-consistent field (SA-CASSCF) method. Core-valence correlations between twenty-four subvalence electrons located on doubly occupied MOs and three valence electrons were implicitly taken into account using a one-electron angular momentum-independent Müller-Mayer core polarization potential (CPP). As a result of topological investigations at over 35,000 points, two dimensional PES, SOC, and ETDM functions were obtained and the geometric parameters Rb_3 were found at which the most intense vertical transitions and the maximum influence of the SOC are expected.

Keywords: ultracold molecules, molecular electronic structure, excited states, spin-orbit coupling, transition probabilities, Rubidium.

DOI: 10.61011/EOS.2023.09.57336.5353-23

Introduction

It has become clear over the past two decades that atoms and molecules of alkali metals are of particular practical importance as model objects for systematic research into fundamental physical and chemical processes occurring at ultralow translational and internal temperatures (i.e., when the quantum properties of an isolated atom or molecule become dominant in the collective behavior of an ultracold atomic–molecular ensemble of such particles). Since the number of internal degrees of freedom and the density of discrete energy levels of molecules are much higher than the corresponding atomic values, laser synthesis, subsequent cooling, and manipulation of molecules at ultralow temperatures still remain rather challenging experimental tasks [1–4]. It is evident that (spectroscopically) accurate data on the energy and radiative properties of molecules within a very wide range of their rovibronic excitation [6] is needed in order to search for optimal pathways for the laser assembly and cooling of polyatomic molecules (and their diatomic counterparts [5]).

The spatial density of particles in a stable ensemble of ultracold molecules produced by laser-induced photoassociation of ultracold atoms this is currently of of the most efficient methods for the synthesis of diatomic molecules at ultralow temperatures [7]) is sufficiently high for atomic–molecular collisions being significant in the context of intramolecular relaxation processes and binary chemical reactions [8]. This is the reason why spatial particle geometries corresponding to a collision between an atom and a forming dimer are considered in a considerable share of theoretical studies focused on the optimization of virtual synthesis of triatomic molecules [9–13]. It bears reminding that triatomic molecules are the last (in terms of the number of atoms) ones for which the calculation of precision 3D potential energy surfaces (PESs) within a wide range of variation of geometrical parameters of a molecule is still worthwhile, since the introduction of additional atoms into quantum-mechanical analysis makes the dimension of the corresponding vibrational-rotational and collisional problem so large that the computational cost of its solution and preliminary detailed scanning over a $(3N\text{-}6)$-dimensional ($N > 3$ is the number of atoms in a molecule) potential energy surface becomes prohibitively high.

The electronic states of a Rb_3 molecule, which were isolated within helium droplets, have been examined spectroscopically in a series of experiments in [1,2,14–17]. Specifically, spin-allowed optical transitions $(2)^4E' \leftarrow (1)^4A_2'$, $(3)^4E' \leftarrow (1)^4A_2'$, $(2)^4E'' \leftarrow (1)^4A_2'$, $(1)^4A_{1,2}' \leftarrow (1)^4A_2''$, and $(1)^2E'' \leftarrow (1)^2E'$ were observed. Already, at the spectra

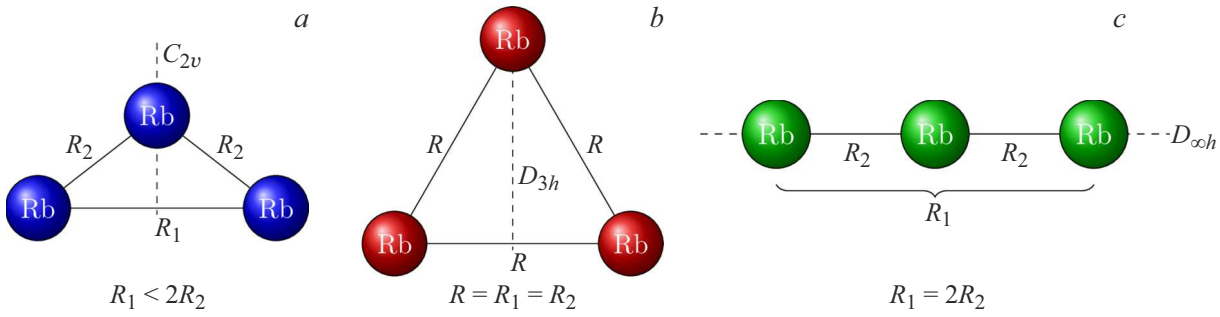

Figure 1. Spatial C_{2v} geometry of a Rb_3 molecule that is in the focus of the present study (*a*). All combinations of interatomic distances $R_1 \leq 2R_2$, including the highly symmetric molecule geometries belonging to point groups (*b*) D_{3h} and (*c*) $D_{\infty h}$, were examined.

assignment stage, only highly symmetric geometries of Rb_3 belonging to the D_{3h} point group were considered.

Owing to the physically feasible high spatial symmetry, homonuclear trimer Rb_3 is a convenient model system for theoretical studies into the Jahn–Teller (JT) effect [18], which manifests in the lowering of the point symmetry of the excited electronic states of the molecule from D_{3h} to C_{2v} (or lower). For example, the two lowest-energy doublet states $(1)^2B_2$ and $(1)^2A_1$ have been examined in detail in [15,19], with the former being the ground state of Rb_3, since they degenerate into a $(1)^2E'$ symmetry state on transition from C_{2v} to a higher D_{3h} symmetry.

The most comprehensive study to date of the energy diagram of electronically excited doublet and quartet states of a Rb_3 molecule has been performed in [13]. However, data on electronic transition dipole moments (ETDMs) and spin-orbit coupling (SOC) in this molecule are still almost completely lacking, although these data are crucial for optimization of multiple cycles of optical assembly, cooling, and manipulation of ultracold Rb_3 molecule ensembles. The principal aim of the present study is to fill this gap.

In the context of quantum-mechanical calculations of the electronic structure, hydrogen-like atoms of alkali metals are distinct in having just a single valence electron. This implies that molecules and even clusters formed exclusively from these atoms may be characterized fairly accurately with explicit correlation of valence electrons only and the residual core-valence correlation taken into account implicitly with the use of a model core polarization potential (CPP) [20,21]. In addition, an effective core potential (ECP), which takes into account at least the scalar relativistic effect, may be used for all electrons lying below the last subvalence shell. Hartree–Fock molecular orbitals (MOs) are then optimized with explicit consideration of the static correlation of valence and subvalence electrons provided by the multi-configuration version of the state-averaged complete active space self-consistent field (SA-CASSCF) method, all subvalence electrons of a molecule are distributed over doubly occupied optimized MOs, and the residual dynamic correlation is taken into account using the multi-reference configuration interaction with singles and doubles (MR-CISD) method for N valence electrons only. Repeated application of this approach [14,21–28] to homonuclear and heteronuclear diatomic molecules of alkali metals has confirmed that it provides fairly accurate results while conserving computational resources.

Details of electronic structure calculations

The overwhelming majority of quantum-mechanical calculations of the electronic structure of the rubidium trimer molecule were performed in the so-called T-shaped spatial geometry with three rubidium atoms forming an isosceles triangle. This geometry characterizes the process of collision between a rubidium dimer molecule (with internuclear distance R_1) and a rubidium atom moving perpendicularly to the interatomic dimer axis and remaining at equal distances R_2 from each dimer atom (Fig. 1). Thus, a Rb_3 molecule belonging to symmetry group C_{2v} was examined in most cases. However, the linear Rb_3 molecule geometry with equal distances between the central atom and two outer atoms, and the highly symmetric equilateral triangle geometry were also included in these calculations. Internuclear distances were scanned from 2 to 10 Å along both coordinates (with the exception of physically infeasible geometries such as $R_1 > 2R_2$). The initial, coarse, PES scan was performed with a pitch of 0.1 Å for both radial coordinates R_1,R_2, the grid pitch within the most intriguing and complex PES regions was then reduced to 0.001 Å. *Ab initio* data for more than 35000 points on the $U(R_1, R_2)$ two-dimensional surface were obtained this way.

The electronic structure of all three rubidium atoms was characterized using the ECP28MDF library basis [29] implemented in the Molpro package [30]. This basis consists of an uncontracted Gaussian set [13s9p5d3f1g] and includes an effective core potential that approximates all electrons (except for a single valence one and eight subvalence electrons) of the Rb atoms with the scalar relativistic effect taken into account. The residual core-valence correlation effect was taken into account using the model Möller–Mayer core polarization potential [20] with the static dipole polarizability of the rubidium ion, α_{Rb^+} set to 9.096 a.u. [31] and cutoff radius $r_c = 0.35$ a.u., which was adjusted so as to

reproduce the experimental energy of the atomic transition $Rb(5s) \rightarrow Rb(5p)$ 12737.34 cm^{-1} [32].

Hartree–Fock molecular orbitals were optimized using the complete active space self-consistent field (CASSCF) method, wherein all electrons in the subvalence shells remained in doubly occupied MOs. In the present case, 24 subvalence electrons of the Rb_3 molecule were positioned in 12 doubly occupied MOs with symmetries $a_1/b_1/b_2/a_2$ (below this order of orbitals is assumed at all times), which correspond to 5/2/4/1 of these shells, respectively. The remaining three valence electrons were located in valence MOs with symmetries 2/0/1/0; in the course of optimization, they were positioned freely in 20 active virtual orbitals (8/5/5/2). The total energy was minimized for all doublet and quartet states that were included initially into the SA-CASSCF procedure.

Wave functions optimized in SA-CASSCF served as a reference space for subsequent characterization of dynamic correlation by the internally contracted multi-reference configuration interaction with singles and doubles (*ic*-MR-CISD) method, wherein all subvalence electrons were frozen in doubly occupied orbitals. PESs for the first 7/4/5/2 doublet states of the corresponding symmetry and the first 5/3/4/2 quartet states were obtained as a result. Multi-reference electronic wave functions were thus used to calculate all possible nonzero ETDM and SOC matrix elements (MEs) within the quasi-relativistic approximation. Note that owing to the use of effective core potentials for characterization of the fine structure of rubidium atoms, the corresponding SOC MEs were calculated within the effective Fock-matrix approximation. All calculations were performed in the Molpro quantum chemistry package [30].

Discussion

Two-dimensional PESs for 32 low-lying doublet and quartet states of the Rb_3 molecule with a T-shaped isosceles triangle geometry were plotted as a result of quantum-chemical calculations of the electronic structure. Stationary points (i.e., the positions of local and global energy minima; see Table 1) and their depths relative to saddle points (Table 2) were determined for all the calculated PESs. Spin-allowed electronic MEs of the electronic transition dipole moment (278 in total) and all allowed (according to the selection rules) spin-orbit coupling MEs (367 in total) were also calculated.

Potential energy surfaces

The results of preliminary (visual) analysis of topology of the obtained 2D potential energy surfaces, ETDMs, and SOC let us draw the following conclusions.

One half of stationary points are localized within a limited range of interatomic distances $R_1 \in [4.367, 5.415]$(Å) and $R_2 \in [4.561, 5.127]$(Å). It bears reminding that the equilibrium distances for triplet and singlet states of the rubidium dimer molecule are 6.188 Å [3] and 4.209 Å [33], respectively. It is evident that the majority of stationary points of the calculated 2D PESs fall within this range [34]; therefore, 1D PES sections of Rb_3 should not differ radically from the potential energy curves of Rb_2.

A number of low-lying electronic terms of the rubidium trimer have two easily identifiable stationary points (see Tables 1 and 2). For example, the $(2)^2A_1$ state PES has two minima: one positioned at point $R_1 = 6.08$ Å, $R_2 = 4.384$ Å and another at $R_1 = 4.199$ Å, $R_2 = 5.164$ Å. The first minimum is positioned approximately 447 cm^{-1} lower than the second one, and the saddle point between them is 917 cm^{-1} above the first minimum and corresponds to the equilateral triangle geometry with internuclear distance of 4.82 Å. The $(4)^2A_1$ term also has two minima at points $R_1 = 4.334$ Å, $R_2 = 5.127$ Å and $R_1 = 5.415$ Å, $R_2 = 4.582$ Å. They are located at approximately the same depth (specifically, 11500 cm^{-1} above the minimum of the $(1)^2B_2$ ground state that is used as a reference point), while the saddle point $R_1 = R_2 = 4.68$ Å is positioned 390 cm^{-1} higher.

It is worth noting that the $(1)^2B_2$ ground doublet term forms a JT pair with the $(1)^2A_1$ state. This means that these states degenerate in calculations in higher symmetry D_{3h} (when the molecule shape is that of an equilateral triangle) and form the ground doublet state of a fully symmetric Rb_3 molecule: $(1)^2E'$. This is seen clearly, e.g., in Fig. 2 that shows PES projections and projections of the difference between PESs (i.e., the energy gap between them). The white triangles in the lower right corner correspond to physical infeasible geometries with $R_1 > 2R_2$. It is evident that the intersection line of PESs of states $(1)^2B_2$ and $(1)^2A_1$ coincides with the $R_1 = R_2$ line (i.e., the D_{3h} geometry). The PES minimum for this line is located at point $R_1 = R_2 = 4.53$ Å with an energy 526 cm^{-1} higher than the minimum energy of the $(1)^2B_2$ state. The results of analysis in lower symmetry C_{2v} reveal that the $(1)^2B_2$ state minimum at point $R_1 = 5.424$ Å, $R_2 = 5.433$ Å lies 147 cm^{-1} lower than the $(1)^2A_1$ state minimum located at point $R_1 = 4.188$ Å, $R_2 = 4.850$ Å.

The coordinates of global PES minima calculated in [13] are also listed in Table 1. For ease of comparison, the data from [13] for states with symmetry B_1 and B_2 are presented directly below the results obtained here for states with symmetry B_2 and B_1, respectively. In general, the positions and energies of stationary points agree well with mean deviations of 0.030 Å, 0.015 Å, and 90 cm^{-1} in R_1, R_2, and energy, respectively. It should be noted that a discrepancy arises in the present study and in [13] in determining which of the two minima for states $(1)^4A_1$ and $(3)^4A_1$ is the global one, although the magnitudes of local and global minima for these two states differ considerably (1795 and 1589 cm^{-1}, respectively). It cannot be said that this discrepancy is caused by insufficient PES scanning in [13], since minima were found there in fairly distant geometries: $R_1 = 8.076$ Å, $R_2 = 4.993$ Å and $R_1 = 7.226$ Å, $R_2 = 4.687$ Å for states $(1)^4A_1$ and $(3)^4A_1$, respectively. However, the authors

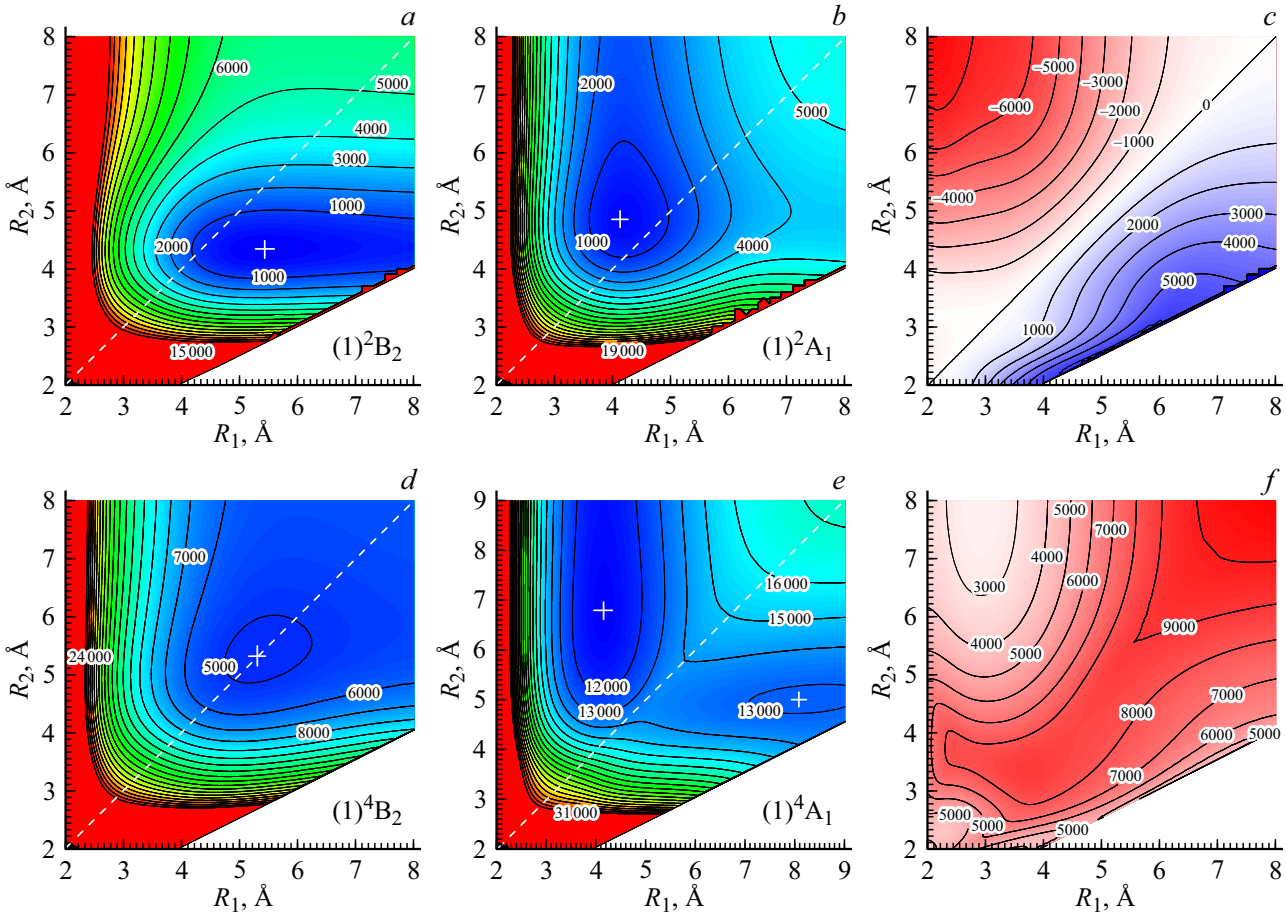

Figure 2. 2D projections of PESs calculated for low-lying doublet and quartet states of the T-shaped Rb_3 molecule (point symmetry group C_{2v}) (*a*,*b*,*d*,*e*) and differences between the corresponding PESs $\Delta E = E_{(1)^2A_1} - E_{(1)^2B_2}$ (*c*) and $\Delta E = E_{(1)^4A_1} - E_{(1)^4B_2}$ (*f*). Here, R_1 is the internuclear distance in the Rb_2 rubidium dimer and R_2 is the distance between a perpendicularly incident Rb atom to dimer atoms. Energies are indicated in inverse centimeters relative to the minimum of the ground electronic state, which turned out to be the $(1)^2B_2$ doublet term. The energy separation between isocurves is 1000 cm^{-1}. White crosses denote the positions of local minima, and the dashed line corresponds to the equilateral triangle geometry (point symmetry group D_{3h}).

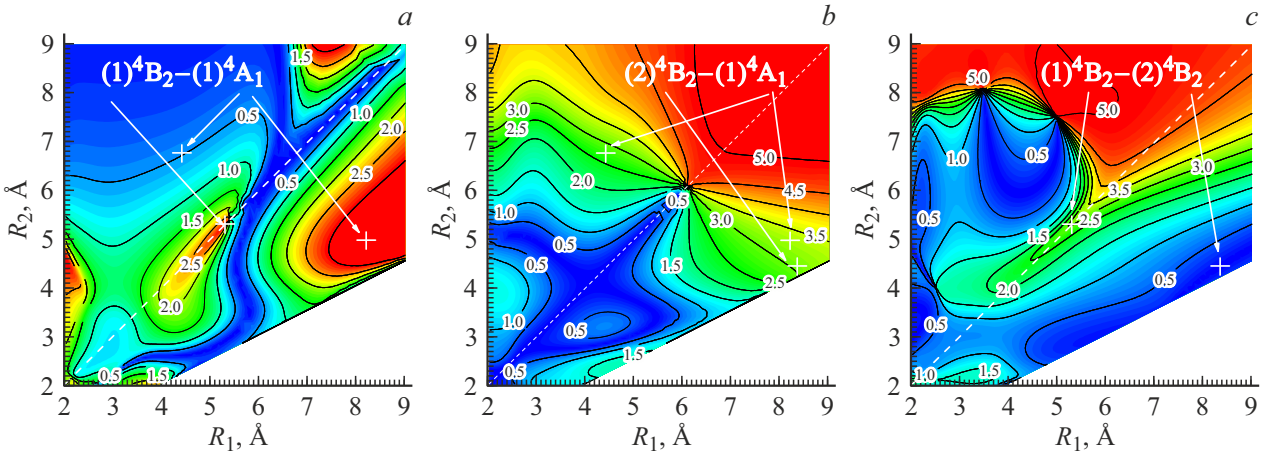

Figure 3. 2D projections of surfaces of spin-allowed electronic matrix elements of the dipole moment of the electronic transition between the $(1)^4B_2$ quartet ground state of the T-shaped Rb_3 molecule and excited states forming Jahn–Teller pair $(1)^4A_1 \sim (2)^4B_2$. Isocurves correspond to absolute values of the matrix element with a pitch of 0.5 a.u. The white crosses denote the positions of local energy minima on the potential energy surfaces of the interacting states. The dashed line corresponds to the equilateral triangle geometry.

Table 1. Positions of local minima of low-lying doublet and quartet states of the T-shaped Rb_3 trimer. Here, R_1 is the interatomic distance in the rubidium dimer, R_2 is the distance between the incident Rb atom and the dimer atoms, and E_{min} is the energy at the potential well minimum relative to the minimum of the $(1)^2B_2$ ground state. PW stands for "Present work"

State	R_1, Å	R_2, Å	E_{min}, cm^{-1}	Source	State	R_1, Å	R_2, Å	E_{min}, cm^{-1}	Source
$(1)^2B_2$	5.424	4.339	0	PW	$(1)^4B_2$	5.311	5.311	4 830	PW
	5.393	4.379	0	[13]		5.311	5.311	4 773	[13]
$(1)^2A_1$	4.188	4.850	147	PW	$(1)^4A_2$	5.731	4.345	9 441	PW
$(1)^2B_1$	4.267	4.267	4 687	PW		5.700	4.368	9 414	[13]
	4.285	4.276	4 789	[13]	$(1)^4B_1$	4.140	4.896	9 681	PW
$(2)^2A_1$	6.080	4.384	6 344	PW	$(2)^4B_2$	8.343	4.417	9 982	PW
	4.199	5.164	6 814	PW		8.179	4.442	9 979	[13]
	6.073	4.398	6 246	[13]	$(1)^4A_1$	4.139	6.791	11 078	PW
$(3)^2A_1$	4.562	4.561	8 081	PW		8.215	4.992	12 873	PW
	4.557	4.557	7 915	[13]		8.076	4.993	12 783	[13]
$(2)^2B_2$	4.815	4.815	7 261	PW	$(2)^4A_1$	5.346	5.344	13 817	PW
$(1)^2A_2$	5.119	4.316	10 319	PW		5.325	5.325	13 739	[13]
	5.132	4.337	10 303	[13]	$(3)^4B_2$	5.088	5.088	14 030	PW
$(2)^2B_1$	4.178	4.730	10 410	PW		5.084	5.084	13 886	[13]
$(4)^2A_1$	4.334	5.127	11 527	PW	$(2)^4B_1$	6.227	4.426	15 636	PW
	5.415	4.582	11 527	PW		4.197	5.466	16 403	PW
$(3)^2B_2$	4.883	4.892	12 177	PW		6.217	4.443	15 507	[13]
$(5)^2A_1$	4.889	4.887	12 178	PW	$(4)^4B_2$	5.371	5.291	16 389	PW
$(4)^2B_2$	5.226	5.226	13 234	PW		5.337	5.283	16 308	[13]
	8.009	4.917	13 453	PW	$(3)^4A_1$	5.277	5.329	16 390	PW
$(6)^2A_1$	4.466	4.466	13 571	PW		7.314	4.714	17 979	PW
$(5)^2B_2$	4.786	4.621	13 856	PW		7.226	4.687	17 801	[13]
$(7)^2A_1$	4.583	4.703	13 858	PW	$(2)^4A_2$	4.884	4.924	17 426	PW
$(2)^2A_2$	5.240	4.463	14 751	PW	$(3)^4B_1$	4.619	4.618	17 734	PW
$(3)^2B_1$	4.366	4.367	14 705	PW	$(4)^4A_1$	4.432	6.320	19 000	PW
	4.259	4.850	14 754	PW		6.178	4.876	19 035	PW
$(4)^2B_1$	4.385	4.616	14 942	PW	$(5)^4A_1$	4.367	5.506	19 477	PW
$(6)^2B_2$	4.730	4.731	15 494	PW		6.451	5.032	20 729	PW
$(8)^2A_1$	4.684	4.952	15 723	PW					

Table 2. Positions of the saddle points (in angstroms) for doublet and quartet states of the T-shaped Rb_3 molecule that feature two relatively deep energy minima in PESs. E is the energy at the saddle point relative to the $(1)^2B_2$ ground state minimum and ΔE_g and ΔE_l are the depths of global and local minima, respectively (in inverse centimeters)

State	R_1	R_2	E	ΔE_g	ΔE_l
$(2)^2A_1$	4.82	4.82	7 261	917	447
$(4)^2A_1$	4.68	4.68	11 917	390	390
$(4)^2B_2$	7.13	4.97	13 649	415	196
$(3)^2B_1$	4.23	4.63	14 778	73	24
$(1)^4A_1$	5.20	4.98	13 683	2605	810
$(2)^4B_1$	4.89	4.89	17 427	1791	1024
$(3)^4A_1$	6.30	4.85	18 549	2159	570
$(4)^4A_1$	5.24	5.15	19 844	844	809
$(5)^4A_1$	5.60	5.06	20 968	1491	239

of [13] failed to find the minima closest to the equilateral triangle geometry, which were revealed in the present study at $R_1 = 4.139$ Å, $R_2 = 6.791$ Å and $R_1 = 5.277$ Å, $R_2 = 5.329$ Å, respectively. Second (local) minima are also observed for terms $(4)^2B_2$, $(3)^2B_1$, $(4)^4A_1$, and $(5)^4A_1$.

Actual values of the PES difference obtained at large internuclear distances (ideally, at the dissociation limit) may be used to estimate roughly the accuracy of the calculated energies of electronic transitions. The overwhelming majority of PESs obtained at $R = R_{1,2} \to \infty$ converge to the dissociation limit corresponding to two rubidium atoms in the ground state and one rubidium atom in the first excited state. Accordingly, test calculations were performed with $R_1 = R_2 = 24.8$ Å for the first seven states of symmetry A_1. The lowest one converges to the ground limit of the rubidium atom, and six excited states converge to the limit corresponding to $2Rb(5s)+Rb(5p)$. Their energies relative to the ground state are 12583, 12592, 12596, 12656, 12660, and 12697 cm^{-1}. Note that the spread of calculated energies is within 115 cm^{-1}. To verify the PES convergence, calculations were also performed at $R = 21, 23, 24$ Å, where the spread was 162, 142, and 126 cm^{-1}, respectively. Greater internuclear distances were

Table 3. Magnitudes of the electronic transition dipole moment and the spin-orbit coupling between lower (1) and upper (2) terms of the Rb_3 molecule at the equilibrium point of lower state (1). ΔE is the energy gap between them at the minimum point of the PES of the first state

Transition (1)	(2)	ETDM, a.u.	SOC, cm^{-1}	ΔE, cm^{-1}	Transition (1)	(2)	ETDM, a.u.	SOC, cm^{-1}	ΔE, cm^{-1}	Transition (1)	(2)	ETDM, a.u.	SOC, cm^{-1}	ΔE, cm^{-1}
$(1)^2B_2$	$(1)^2A_1$	0.609	15.413	2 471	$(1)^2A_1$	$(2)^2A_1$	1.239	–	6 806	$(1)^4B_2$	$(1)^2A_1$	–	0.328	-3 019
	$(2)^2A_1$	0.731	2.921	6 576		$(3)^2A_1$	1.962	–	8 933		$(2)^2A_1$	–	0.240	2 922
	$(3)^2A_1$	0.775	4.671	9 867		$(4)^2A_1$	4.550	–	11 507		$(3)^2A_1$	–	4.627	4 573
	$(4)^2A_1$	0.840	14.099	11 704		$(5)^2A_1$	1.080	–	12 974		$(4)^2A_1$	–	0.481	7 611
	$(5)^2A_1$	1.163	6.711	13 685		$(6)^2A_1$	1.005	–	13 903		$(5)^2A_1$	–	5.367	7 782
	$(6)^2A_1$	1.958	4.754	14 596		$(7)^2A_1$	0.106	–	14 029		$(6)^2A_1$	–	0.146	9 922
	$(7)^2A_1$	3.063	0.078	14 741		$(8)^2A_1$	0.562	–	15 976		$(7)^2A_1$	–	1.784	10 752
	$(8)^2A_1$	3.644	0.941	16 462	$(1)^2A_1$	$(1)^2B_1$	0.055	30.404	5 352		$(8)^2A_1$	–	0.166	11 368
$(1)^2B_2$	$(1)^2B_1$	–	27.959	5 925		$(2)^2B_1$	0.926	8.654	10 283	$(1)^4B_2$	$(1)^2B_1$	–	0.230	2 980
	$(2)^2B_1$	–	11.386	1 2435		$(3)^2B_1$	2.079	7.910	14 615		$(2)^2B_1$	–	0.304	7 366
	$(3)^2B_1$	–	6.579	1 5435		$(4)^2B_1$	1.837	4.354	15 101		$(3)^2B_1$	–	1.478	11 120
	$(4)^2B_1$	–	4.838	1 6634	$(1)^2A_1$	$(1)^2B_2$	0.385	15.932	1 485		$(4)^2B_1$	–	0.059	12 211
$(1)^2B_2$	$(2)^2B_2$	0.574	–	7 971		$(2)^2B_2$	0.400	3.525	7 563	$(1)^4B_2$	$(1)^2B_2$	–	–	-3 013
	$(3)^2B_2$	3.889	–	12 836		$(3)^2B_2$	2.625	13.025	12 518		$(2)^2B_2$	–	–	2 922
	$(4)^2B_2$	1.968	–	14 041		$(4)^2B_2$	3.655	2.190	13 965		$(3)^2B_2$	–	–	7 610
	$(5)^2B_2$	2.087	–	14 435		$(5)^2B_2$	1.660	5.600	14 122		$(4)^2B_2$	–	–	8 412
	$(6)^2B_2$	0.681	–	16 302		$(6)^2B_2$	1.236	2.922	15 793		$(5)^2B_2$	–	–	9 924
$(1)^2B_2$	$(1)^2A_2$	1.227	7.434	10 343	$(1)^2A_1$	$(1)^2A_2$	–	8.804	11 521		$(6)^2B_2$	–	–	11 314
	$(2)^2A_2$	1.156	7.644	14 814		$(2)^2A_2$	–	6.295	15 790	$(1)^4B_2$	$(1)^2A_2$	–	2.672	7 372
$(1)^2B_2$	$(1)^4A_1$	–	0.377	14 171	$(1)^2A_1$	$(1)^4A_1$	–	–	12 496		$(2)^2A_2$	–	3.071	11 125
	$(2)^4A_1$	–	0.706	16 134		$(2)^4A_1$	–	–	15 111	$(1)^4B_2$	$(1)^4A_1$	3.038	0.093	8 908
	$(3)^4A_1$	–	2.891	18 808		$(3)^4A_1$	–	–	17 575		$(2)^4A_1$	0.869	4.835	8 988
	$(4)^4A_1$	–	5.142	19 814		$(4)^4A_1$	–	–	19 369		$(3)^4A_1$	0.518	0.002	11 563
	$(5)^4A_1$	–	10.745	21 913		$(5)^4A_1$	–	–	20 100		$(4)^4A_1$	0.689	0.037	15 029
$(1)^2B_2$	$(1)^4B_1$	–	4.351	12 447	$(1)^2A_1$	$(1)^4B_1$	–	3.200	9 541		$(5)^4A_1$	0.076	0.037	15 801
	$(2)^4B_1$	–	16.755	16 235		$(2)^4B_1$	–	15.705	16 666	$(1)^4B_2$	$(1)^4B_1$	–	17.857	6 727
	$(3)^4B_1$	–	7.800	19 289		$(3)^4B_1$	–	8.828	18 755		$(2)^4B_1$	–	12.247	12 850
$(1)^2B_2$	$(1)^4B_2$	–	–	5 982	$(1)^2A_1$	$(1)^4B_2$	–	2.466	5 611		$(3)^4B_1$	–	0.061	13 713
	$(2)^4B_2$	–	–	11 953		$(2)^4B_2$	–	2.712	14 081	$(1)^4B_2$	$(2)^4B_2$	3.042	–	8 917
	$(3)^4B_2$	–	–	15 557		$(3)^4B_2$	–	1.113	15 396		$(3)^4B_2$	0.018	–	9 303
	$(4)^4B_2$	–	–	17 980		$(4)^4B_2$	–	1.730	17 661		$(4)^4B_2$	4.664	–	11 564
$(1)^2B_2$	$(1)^4A_2$	–	2.987	9 463	$(1)^2A_1$	$(1)^4A_2$	–	0.291	11 263	$(1)^4B_2$	$(1)^4A_2$	0.001	10.273	6 736
	$(2)^4A_2$	–	12.194	18 041		$(2)^4A_2$	–	19.505	17 725		$(2)^4A_2$	0.006	7.078	12 849

not tested in calculations due to SA-CASSCF convergence issues. Thus, it is fair to say that the PES differences converge roughly to an energy of 12630 cm^{-1}, which is just 105 cm^{-1} (approximately 1%) lower than the experimental value of the atomic excitation energy.

Functions of electronic transition dipole moments

As was expected, the ETDM magnitudes determined for Rb_3 fall mostly within the interval typical of the corresponding parameters observed both in an Rb_2 diatomic molecule and in an isolated rubidium atom. It is worth reminding that the experimental ETDM value for the $5^2S - 5^2P$ electronic transition is 3.16 a.u. in an isolated rubidium atom [32]. The median value for 85% of the obtained Rb_3 ETDM surfaces does not exceed 1.0 a.u., while most of the remaining 15% reach the maximum atomic value. The highest ETDM values correspond to the transitions between terms $(3)^2A_1$ and $(1)^2B_1$: the maximum and median values for them are 5.36 and 3.70 a.u., respectively.

The ETDM values for vertical transitions between the ground and excited states of the examined trimer appear to be of the most interest in terms of their future application to optimization of laser cooling cycles and manipulation of ultracold Rb_3 molecule ensembles. The absolute ETDM ME values for spatial geometries corresponding to the PES minima for the ground terms (as a reminder, these are the $(1)^4A_1 \sim (2)^4B_2$ Jahn–Teller pair and the $(1)^4B_2$ ground quartet state) are listed in Table 3. The energy differences between the corresponding PESs for the same geometries are also presented there. Dashes denote those state pairs that have a zero ETDM value due to spin or symmetry forbiddenness of combining states.

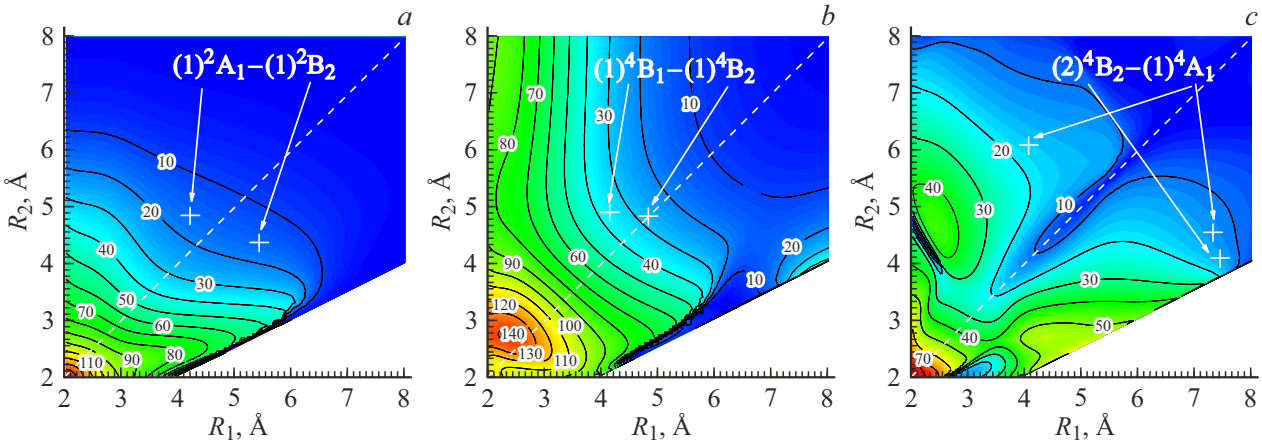

Figure 4. 2D projections of the surface of electronic matrix elements of spin-orbit coupling obtained for low-lying doublet and quartet pairs of interacting states of the Rb_3 molecule. Isocurves are spaced by 10 cm^{-1}. White crosses denote the positions of minima on the PESs of interacting states, and the dashed line corresponds to the equilateral triangle geometry.

State $(1)^4A_2$ is the closest in energy to the ground quartet one among those that have a nonzero component of the ETDM operator. The dipole moment of the transition to it is small not only at an equilibrium geometry of state $(1)^4B_2$, but also within effectively the entire coupled region of the Rb_3 molecule. The ETDM function value for this transition exceeds 0.5 a.u. only when $R_2 > 8$ Å and $R_1 \in (2, 7)$ Å. The range of geometries corresponds to an Rb atom incident perpendicularly onto an Rb_2 molecule. It turned out that the ETDM value for the next (in terms of energy) state $(1)^4A_1$ is fairly significant: 3.038 a.u. at an equilibrium geometry of the ground quartet state. However, this transition cannot be examined individually, since the PESs of states $(1)^4A_1$, $(2)^4A_1$, and $(2)^4B_2$ intersect at these geometries. Figure 3 shows the projections of dipole moments of electronic transitions between the $(1)^4B_2$ ground quartet state and states $(1)^4A_1$ and $(2)^4B_2$ (the dipole moment of the transition to the ground quartet state for them is somewhat greater than to $(2)^4A_1$; see Table 3). Note that states $(1)^4A_1$ and $(2)^4B_2$ have closely positioned stationary points (local minimum for $(1)^4A_1$ and global minimum for $(2)^4B_2$), and the ETDM value in the vicinity of the common PES is greater than 3 a.u. It is also seen clearly in Fig. 3 that the ETDM within this pair of states remains low both at an equilibrium geometry of the ground state and at shorter internuclear distances, rising steeply when R_1 or R_2 exceed 6 Å. The ETDM value is also small in the vicinity of the global minimum of state $(1)^4A_1$, remaining below 0.5 a.u.; in contrast, the ETDM at the local minimum exceeds 3 a.u.

Spin-orbit coupling functions

To conclude, let us examine certain peculiarities of the results of calculation of the spin-orbit coupling ME in Rb_3. Just as in the case of ETDM, the SOC magnitude in Rb_3 remains comparable to the SOC value observed in an isolated atom and an Rb_2 dimer. It is worth reminding here that the SOC magnitude for a rubidium atom is $\xi^{so}_{Rb} = [E_{5^2P_{3/2}} - E_{5^2P_{1/2}}]/3 = 79$ cm^{-1} [32]. Accordingly, the magnitude of SOC matrix elements in the coupled region of the Rb_2 dimer without the inclusion of self-consistent coefficients for reproducing the spin-orbit splitting at the dissociation limit (see [35] for details) typically falls within the range from 30 to 80 cm^{-1} [26]. This is not the case for the examined rubidium trimer. Although several pairs of states with the values of molecular SOC MEs exceeding 100 cm^{-1} do exist, multiple pairs of states have SOC matrix elements remaining below 20 cm^{-1} in most examined geometries. It follows from Table 3 that only 15 pairs have SOC magnitudes above 10 cm^{-1} at an equilibrium geometry of ground states, and only two states interact with an energy higher than 20 cm^{-1}. The SOC surfaces for these two states are shown in Figs. 4, *a*,*b*. Figure 4, *a* illustrates SOC in the doublet JT pair. The SOC surface for the $(1)^4B_1$–$(1)^4A_2$ quartet JT pair is roughly similar to the one for the doublet JT pair but compressed with a coefficient close to 2/3. Thus, it reaches a lower value of approximately 100 cm^{-1} (instead of 150 cm^{-1}) when all three atoms converge to a distance of 2 Å. At the minimum positions of states $(1)^4A_2$ and $(1)^4B_1$, the magnitude of SOC between them is approximately equal to 7 cm^{-1}. It is seen clearly in Fig. 4 that SOC values of 80 cm^{-1} and above are generally found only in extreme geometries where atoms converge to very close distances. Examining the corresponding PESs in Fig. 2, one finds that compression of the trimer to internuclear distances shorter than 3 Å comes with a colossal energy cost. Thus, it is fair to say that the mean SOC magnitude in Rb_3 is on the order of 15 cm^{-1} for most states and geometries, and only certain select pairs of interacting states (e.g., $(1)^4B_1$–$(1)^4B_2$) have SOC values above 30 cm^{-1}. Figure 4, *c* shows the 2D sections of SOC surfaces for the pair of intersecting states $(1)^4A_1$–$(2)^4B_2$; one can readily see a region of weaker SOC, which is especially pronounced

around the equilateral triangle geometry within the region of variation of internuclear distances from $R_1 = R_2 = 3.5$ Å to approximately $R_1 = R_2 = 6.5$ Å.

Conclusion

Comprehensive quantum-chemical calculations of the electronic structure were performed to find potential energy surfaces and matrix elements of the electronic transition dipole moment and spin-orbit coupling for certain low-lying doublet and quartet states of a homonuclear rubidium trimer. The obtained PESs were subjected to initial analysis: stationary points (positions of local and global minima) and the positions of saddle points were determined. The Rb_3 molecule proved to be a fine model system for the examination of the Jahn–Teller effect, which is observed for the ground doublet state and the first excited quartet state of this molecule. The geometric parameters of Rb_3 presumably allowing for the most intense vertical transitions and the most vivid manifestations of the spin-orbit effect were identified by examining the topology of two-dimensional PES, ETDM, and SOC functions calculated at more than 35000 points. The obtained *ab initio* data may eventually be used in the search for optimum methods for the laser synthesis, cooling, and manipulation of stable ensembles of Rb_3 molecules at ultralow temperatures.

It is worth emphasizing in conclusion that the accuracy of U^{ground} PES determination for the ground doublet and quartet state may be enhanced considerably in alternative multi-reference and/or single-reference cluster calculations (MR-AQCC and CCSD(T), respectively) with the basis set superposition error (BSSE) and the basis finiteness taken into account by extrapolating the results to a complete basis set (CBS). The corresponding U^{exc} PESs of excited states may then also be refined significantly by applying an *a posteriori* procedure [36] based on the presumed compensation of the greater part of the systematic quantum-mechanical calculation error in the so-called "difference-based" potential $\Delta U = U^{\text{exc}}_{\text{CISD}} - U^{\text{ground}}_{\text{CISD}}$:

$$U^{\text{exc}}_{\text{corr}} = U^{\text{ground}}_{\text{CCSD(T)/BSSE/CBS}} + \Delta U.$$

Funding

This study was supported by grant No. 22-73-00095 from the Russian Science Foundation, https://rscf.ru/project/22-73-00095/.

Conflict of interest

The authors declare that they have no conflict of interest.

References

[1] C. Giese, F. Stienkemeier, M. Mudrich, A.W. Hauser, W.E. Ernst. Phys. Chem. Chem. Phys., **13** (42), 18769–18780 (2011). DOI: 10.1039/c1cp21191a

[2] A.W. Hauser, W.E. Ernst. Phys. Chem. Chem. Phys., **13** (42), 18762–18768 (2011). DOI: 10.1039/c1cp21163c

[3] P. Soldan. J. Chem. Phys., **132** (23), 234–308 (2010). DOI: 10.1063/1.3455710

[4] A.W. Hauser, J.V. Pototschnig, W.E. Ernst. Chem. Phys., **460**, 2–13 (2015). DOI: 10.1016/j.chemphys.2015.07.027

[5] E.A. Pazyuk, A.V. Zaitsevskii, A.V. Stolyarov, M. Tamanis, R. Ferber. Russian Chemical Reviews, **84** (10), 1001 (2015). DOI: 10.1070/RCR4534

[6] I. Klincare, O. Nikolayeva, M. Tamanis, R. Ferber, E.A. Pazyuk, A.V. Stolyarov. Phys. Rev. A, **85**, 062520 (2012). DOI: 10.1103/PhysRevA.85.062520

[7] A.Stolyarov. *Laser Synthesis of Ultra-Cold Molecules: From Design to Production* (Springer International Publishing, 2017), pp. 169177. DOI: 10.1007/978-3-319-52431-3_16

[8] A.A. Buchachenko, A.V. Stolyarov, M.M. Szczesniak, G. Chałłasinski. J. Chem. Phys., **137** (11), 114305 (2012). DOI: 10.1063/1.4752740

[9] M. Tomza, K.W. Madison, R. Moszynski, R.V. Krems. Phys. Rev. A, **88**, 050701(R) (2013). DOI: 10.1103/PhysRevA.88.050701

[10] P. Jasik, J. Kozicki, T. Kilich, J.E. Sienkiewicz, N.E. Henriksen. Phys. Chem. Chem. Phys., **20** (27), 18663–18670 (2018). DOI: 10.1039/c8cp02551g

[11] M.D. Frye, J.M. Hutson. New J. Phys., **23** (12), 125008 (2021). DOI: 10.1088/1367-2630/ac38

[12] P.D. Gregory, M.D. Frye, J.A. Blackmore, E.M. Bridge, R. Sawant, J.M. Hutson, S.L. Cornish. Nat. Commun., **10** (1), 3104 (2019). DOI: 10.1038/s41467-019-11033-y

[13] J. Schnabel, T. Kampschulte, S. Rupp, J.H. Denschlag, A. Kohn. Phys. Rev. A, **103** (2), 022820 (2021). DOI: 10.1103/PhysRevA.103.022820

[14] G. Aubock, J. Nagl, C. Callegari, W.E. Ernst. J. Chem. Phys., **129** (11), 1–10 (2008). DOI: 10.1063/1.2976765

[15] A.W. Hauser, G. Aubock, C. Callegari, W.E. Ernst. J. Chem. Phys., **132** (16), 164310 (2010). DOI: 10.1063/1.3394015

[16] J. Nagl, G. Aubock, A.W. Hauser, O. Allard, C. Callegari, W.E. Ernst. J. Chem. Phys., **128** (15), 1–9 (2008). DOI: 10.1063/1.2906120

[17] J. Nagl, G. Aubock, A.W. Hauser, O. Allard, C. Callegari, W.E. Ernst. Phys. Rev. Lett., **100** (6), 1–4 (2008). DOI: 10.1103/PhysRevLett.100.063001

[18] I.B. Bersuker. *The Jahn-Teller Eect and Vibronic Interactions in Modern Chemistry. Modern Inorganic Chemistry* (Plenum Press, New York, 1984), p. 371. DOI: 10.1007/978-1-4613-2653-3

[19] A.W. Hauser, C. Callegari, P. Soldan, W.E. Ernst. Chem. Phys., **375** (1), 73–84 (2010). DOI: 10.1016/j.chemphys.2010.07.025

[20] W. Muller, J. Flesch, W. Meyer. J. Chem. Phys., **80**, 3297 (1984). DOI: 10.1063/1.447083

[21] E.A. Bormotova, S.V. Kozlov, E.A. Pazyuk, A.V. Stolyarov. Phys. Chem. Chem. Phys., **20** (3), 1889–1896 (2018). DOI: 10.1039/C7CP05548J

[22] S.V. Kozlov, E.A. Bormotova, A.A. Medvedev, E.A. Pazyuk, A.V. Stolyarov, A. Zaitsevskii. Phys. Chem. Chem. Phys., **22**, 2295–2306 (2020). DOI: 10.1039/C9CP06421D

[23] E.A. Bormotova, S.V. Kozlov, E.A. Pazyuk, A.V. Stolyarov, I. Majewska, R. Moszynsky. Phys. Chem. Chem. Phys., **23** (9), 5187–5198 (2021). DOI: 10.1039/D0CP06487D

[24] E.A. Bormotova, S.V. Kozlov, E.A. Pazyuk, A.V. Stolyarov, W. Skomorowski, I. Majewska, R. Moszynski. Phys. Rev. A, **99** (1), 12507 (2019). DOI: 10.1103/PhysRevA.99.012507
[25] E.A. Pazyuk, E. Revina, A.V. Stolyarov. JQSRT, **177**, 283–290 (2016). DOI: 10.1016/j.jqsrt.2016.01.004
[26] E.A. Pazyuk, E.I. Revina, A.V. Stolyarov. Chem. Phys., **462**, 51–56 (2015). DOI: 10.1016/j.chemphys.2015.07.018
[27] V. Krumins, A. Kruzins, M. Tamanis, R. Ferber, V.V. Meshkov, E.A. Pazyuk, A.V. Stolyarov, A. Pashov. J. Chem. Phys., **156** (11), 114305 (2022). DOI: 10.1063/5.0082309
[28] V. Krumins, A. Kruzins, M. Tamanis, R. Ferber, A. Pashov, A.V. Oleynichenko, A. Zaitsevskii, E.A. Pazyuk, A.V. Stolyarov. JQSRT, **256**, 107291 (2020). DOI: 10.1016/j.jqsrt.2020.107291
[29] I.S. Lim, P. Schwerdtfeger, B. Metz, H. Stoll. J. Chem. Phys., **122** (10), 104103 (2005). DOI: 10.1063/1.1856451
[30] H. Werner, P. Knowles, G. Knizia, F. Manby, M. Schutz, P. Celani, T. Korona, R. Lindh, A. Mitrushenkov, G. Rauhut, et al. Molpro, version 2010.1, a package of ab initio programs (2010). ihttp://www.molpro.net
[31] J. Mitroy, M.S. Safronova, C.W. Clark. J. Phys. B, **43** (20), 202001 (2010). DOI: 10.1088/0953-4075/43/20/202001
[32] A. Kramida, Yu. Ralchenko, J. Reader, and NIST ASD Team. NIST Atomic Spectra Database, [https://physics.nist.gov/asd]. NIST, Gaithersburg, MD. (2023)
[33] J.Y. Seto, R.J. Le Roy, J. Vergés, C. Amiot. J. Chem. Phys., **113** (8), 3067–3076 (2000). DOI: 10.1063/1.1286979
[34] W. Jastrzebski, P. Kowalczyk, J. Szczepkowski, A.R. Allouche, P. Crozet, A.J. Ross. J. Chem. Phys., **143** (4), 044308 (2015). DOI: 10.1063/1.4927225
[35] H. Kato. B. Chem. Soc. Jpn., **66** (11), 3203–3234 (1993). DOI: 10.1246/bcsj.66.3203
[36] A. Zaitsevskii, E.A. Pazyuk, A.V. Stolyarov, O. Docenko, I. Klincare, O. Nikolayeva, M. Auzinsh, M. Tamanis, R. Ferber. Phys. Rev. A, **71** (1), 012510 (2005). DOI: 10.1103/PhysRevA.71.012510

Translated by D.Safin